Phase distribution and amplitude of a micromaser field in a semiclassical approximation

Jozef Skvarcek and Mark Hillery
Department of Physics and Astronomy, Hunter College of CUNY, 695 Park Avenue, New York, New York 10021
(Received 8 November 1999; published 13 June 2000)

We present a semiclassical method for determining the phase distribution and the average photon number of a steady-state micromaser field pumped by a stream of resonant two-level atoms in a superposition of their upper and lower states. Assuming the field to have a photon number distribution with a single sharp peak, we find an equation for the amplitude and the phase of the steady-state field, which has two solutions. The stability analysis shows which one of the two is physically realizable. Using the very simple time evolution of particular atomic states, valid in the semiclassical limit, we find an expression for the phase distribution of the field that contains the mean photon number as a parameter. That can be determined from the stable solution.

PACS number(s): 42.50.Dv

I. INTRODUCTION

A micromaser is a very simple physical system that consists of a beam of two-level atoms and a single-mode electromagnetic field within a microwave cavity. Despite its simplicity and the fact that it has been the object of vigorous research for more than a decade, it still presents a researcher with new challenges.

Filipowicz *et al.* in 1986 published some papers on the theory of the microscopic maser [1,2]. They investigated the steady-state cavity field and they found that as the pump rate increased, it goes through thresholds that resemble first-order phase transitions [3]. Guzman *et al.* worked out the semiclassical theory, and they found that the system at a threshold undergoes a transition from one branch of the semiclassical solution to the next [4]. Progress was made not only in the theoretical understanding of the system, but also, around the same time, advances in experimental physics made it possible to build superconducting high-Q microcavities, so that the field could maintain large average photon number, which combined with Rydberg-state spectroscopy, made real micromaser experiments possible. Experiments conducted at the Max Planck Institute for Quantum Optics in Garching have confirmed theoretical predictions of such quantum phenomena as sub-Poissonian photon statistics, quantum Rabi oscillations, and quantum collapses and revivals [5–8].

Most of the studies of the dynamics of the micromaser have considered only injected atoms in their upper states, while the situation in which the atoms enter the cavity in a coherent superposition of their upper and lower states has received far less attention. The micromaser with injected atomic coherence has been investigated by several authors. Krause *et al.*, assuming weak atom-field coupling, found that the phase of the atomic coherence is transferred to the micromaser field and that the excitation probability of the atoms leaving the microwave cavity depends on the relative phase angle between incoming atom dipoles and the field [9]. Since the outgoing atoms are available for measurement, an experiment could be set up to determine the coherence of the field. Slosser *et al.* studied lossless micromaser with coherent pumping and they found that the field evolves towards pure states, which were named tangent and cotangent states [10–12]. These states rely on the existence of trapping states, and apart from having other nonclassical properties, they can be used for generating macroscopic quantum superpositions. The authors also numerically investigated the situation when the state of the field consists of a tangent state and a cotangent state in adjacent blocks of number states. This leads to the occurrence of the interesting period-2 oscillations when the steady-state field returns to its initial value not after interaction with one, but after two atoms. A simple physical explanation of this phenomenon was found by Hillery *et al.* [13]. The effect of the atomic phase was also studied for a multinode laser system; Kien *et al.* developed the quantum theory of the two-mode Λ laser with atoms injected in a superposition of their states [14].

The case in which the atoms are in a coherent superposition is a more complicated problem than the case in which they are completely inverted. In the latter case, the diagonal elements of the density matrix couple only to each other, but when there is atomic coherence this is no longer the case. The entire density matrix must be treated at once. At the same time this is also a more interesting problem since the atomic dipoles have a phase, and because they drive the field, the field has a phase as well. The steady-state field produced by atoms in their upper states has no mean phase, because any value of the phase is equally likely.

Here we want to extend the semiclassical approximation to the micromaser with injected atomic coherence. In particular, our objective is to determine mean photon number and the phase distribution, of the steady-state field. We present a short review of the micromaser system in Sec. II, and Sec. III includes the core of our semiclassical treatment. We find an equation for the amplitude and the phase of the steady-state field, which can be solved and has two solutions. In order to determine which one is physically realizable, we perform a stability analysis in Sec. IV. Then we turn our attention to the problem of finding an approximate expression for the phase distribution of the field in Sec. V. We employ techniques developed by Gea-Banacloche to treat the problem [15]. These rely on the very simple time evolution of particular atomic states. We are able to use them to find an expression for the phase distribution, which contains the mean photon number as a parameter. Our analytical results are compared to quantum-mechanical numerical simulations in Sec. VI, and we find that the agreement is very good.

II. MICROMASER

We shall begin by describing briefly the micromaser. A micromaser consists of a beam of two-level atoms passing through a high-Q microwave cavity containing an electromagnetic field. It is assumed that the atomic beam is of low density, i.e., at any given time there is at most one atom present in the cavity. We also assume that the microcavity supports only one mode of the field, which is in resonance with the atoms at the frequency ω and that the atoms have all the same velocity, so that they pass through the cavity in a constant time τ. The atom-field interaction is governed by the Jaynes-Cummings Hamiltonian, and when the cavity is empty, the field decays into the environment, which is in our case at zero temperature. If the probability of the atoms being in their upper states is high when they enter the microcavity, then the micromaser can maintain a nonzero steady-state field.

The atoms have states $|a\rangle$, with energy ω (we are using units with $\hbar=1$), and $|b\rangle$, with energy 0. The Hamiltonian describing the atom-field system is

$$H=\omega a^{\dagger}a+\frac{1}{2}\omega(\sigma_3+I)+g(a^{\dagger}\sigma^{-}+a\sigma^{+}), \tag{1}$$

where a, $a^{\dagger}$ are the annihilation and creation Bose operators for the field obeying the standard commutation relations

$$[a^{\dagger},a]=1,[a,a]=[a^{\dagger},a^{\dagger}]=0, \tag{2}$$

σ_3 and $\sigma^{\pm}$ are the Pauli spin operators, σ^{+} is raising atomic operator, $\sigma^{+}|b\rangle=|a\rangle$, σ^{-} is lowering operator, $\sigma^{-}|a\rangle=|b\rangle$, and g is the atom-field interaction constant. The first two terms on the right-hand side of Eq. (1) describe free field and free atom, respectively, while the third is the atom-field interaction. The Hamiltonian is given in the rotating-wave approximation. If the atom is initially in the state

$$|\Psi_{\mathrm{at}}\rangle=\alpha|a\rangle+\beta|b\rangle, \tag{3}$$

where α and β are complex numbers satisfying the normalization condition $|\alpha|^2+|\beta|^2=1$, and the field is initially in the state

$$|f\rangle=\sum_{n=0}^{\infty} d_n|n\rangle, \tag{4}$$

then after a time τ the state of the combined system will be

$$|f\rangle\otimes(\alpha|a\rangle+\beta|b\rangle)\rightarrow\sum_{n=0}^{\infty} d_n(\alpha c_{n+1}|n\rangle-\mathrm{i}\beta s_n|n-1\rangle)|a\rangle + \sum_{n=0}^{\infty} d_n(\beta c_n|n\rangle-\mathrm{i}\alpha s_{n+1}|n+1\rangle)|b\rangle, \tag{5}$$

where

$$s_n=\sin(g\tau\sqrt{n})=\sin(\theta_{\mathrm{int}}\sqrt{n/N_{ex}}), \tag{6}$$

$$c_n=\cos(g\tau\sqrt{n})=\cos(\theta_{\mathrm{int}}\sqrt{n/N_{\mathrm{ex}}}). \tag{7}$$

Here, we have introduced the pumping parameter $\theta_{\mathrm{int}}=\sqrt{N_{\mathrm{ex}}}\,g\tau$. The number N_{ex} is the mean number of atoms interacting with the cavity field during its lifetime. Equation (5), which is written in the interaction picture defines the Jaynes-Cummings time evolution of the field density matrix $\hat{\rho}=\mathrm{Tr}_{\mathrm{at}}\hat{\rho}_{\mathrm{system}}$, which can be written formally as $\hat{\rho}(\tau)=M\hat{\rho}(0)$, and in the number-state representation we have

$$\rho_{nm}\rightarrow\rho_{nm}(|\alpha|^2c_{n+1}c_{m+1}+|\beta|^2c_nc_m)+\rho_{n-1,m-1}|\alpha|^2s_ns_m + \rho_{n+1,m+1}|\beta|^2s_{n+1}s_{m+1}+\mathrm{i}\alpha\beta^{*}(c_{n+1}s_{m+1}\rho_{n,m+1} - s_nc_m\rho_{n-1,m})+i\alpha^{*}\beta(c_ns_m\rho_{n,m-1} - s_{n+1}c_{m+1}\rho_{n+1,m}), \tag{8}$$

where $\rho_{nm}=\langle n|\hat{\rho}|m\rangle$. As one can see, the interaction couples together elements from different diagonals, which makes its analysis complicated. In the case of noncoherent pumping, $|\alpha\beta|=0$, only the diagonal terms are coupled.

The decay of the micromaser field for the cavity at zero temperature, formally given as $\hat{\rho}(t)=\mathrm{e}^{Lt}\hat{\rho}(0)$, is described by the master equation [16]

$$\frac{d\hat{\rho}}{dt}=L\hat{\rho}=-\frac{1}{2}\gamma(a^{\dagger}a\hat{\rho}+\hat{\rho}a^{\dagger}a-2a\hat{\rho}a^{\dagger}), \tag{9}$$

which has the solution in the number-state representation

$$\rho_{mn}(t)=e^{-\gamma t(m+n)/2}\sum_{l=0}^{\infty}\left(\frac{(m+l)!}{m!}\,\frac{(n+l)!}{n!}\right)^{1/2} \times\frac{(1-e^{-\gamma t})^l}{l!}\rho_{m+l,n+l}(0), \tag{10}$$

where γ is the loss coefficient. Its reciprocal $1/\gamma$ is equal to the mean cavity lifetime.

The times the pumping atoms arrive into the microwave cavity may conform to various distributions. For the case when they obey Poissonian statistics we can derive the equation of motion for the average field density matrix in the form of a master equation [1]

$$\frac{d\hat{\rho}}{dt}=r(M-1)\hat{\rho}+L\hat{\rho}, \tag{11}$$

where r denotes the mean rate the atoms arrive at the cavity, and it is related to N_{ex} by $N_{\mathrm{ex}}=r/\gamma$. Equation (11) can be employed for finding the steady-state field density matrix by putting $d\hat{\rho}/dt=0$. On the other hand, when considering a regularly pumped micromaser, i.e., when the time T between two consecutive atoms is constant, the time evolution of the field density matrix is given by the map

$$\hat{\rho}(t_{i+1})=e^{LT}M\hat{\rho}(t_i). \tag{12}$$

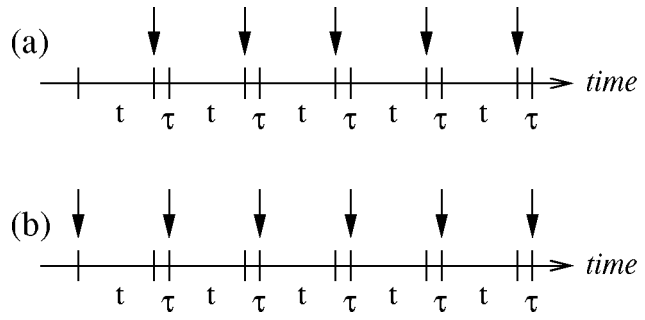

FIG. 1. The time scale for the regularly pumped micromaser. The atom-field interaction time τ is much smaller then the time interval between two consecutive atoms t. The field can be measured just before the next atom enters the cavity, the arrows in (a), or after just after the interaction (b), for example.

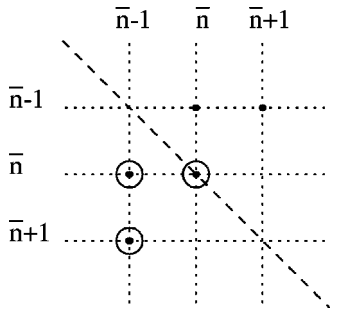

FIG. 2. Relevant part of the field density matrix assumed in the semiclassical treatment. The dashed line represents the main diagonal, the field is strongly peaked around $\rho_{\bar{n}\bar{n}}$. In order to determine $\langle a\rangle$ also $\rho_{\bar{n},\bar{n}-1}$ and $\rho_{\bar{n}+1,\bar{n}-1}$ are needed, other elements are neglected.

If t_i are the times the atoms enter the cavity, $t_{i+1}-t_i=T$. The steady state is usually defined for this case as $\hat{\rho}(t_{i+1})=\hat{\rho}(t_i)=\rho_{ss}$, which says that the field density matrix is the same at any of the times just before an atom enters the cavity, see Fig. 1(a). Of course, the density matrix could be different if measured not at t_i's, we would have different ρ_{ss} should we measure the cavity field at the times just after the atom-field interaction, for example, Fig. 1(b).

It is possible to study the micromasers whose pumping statistics lies somewhere between the regular and Poissonian statistics [17,18], but such cases will not be considered here.

III. SEMICLASSICAL APPROXIMATION

The objective in this section is to find the equation of motion for the amplitude and the phase of the micromaser field, which will later enable us to determine the steady-state values of these quantities. We will assume that the atomic pumping statistics is Poissonian. We will also assume that the steady-state field has a large amplitude, and that its photon number distribution is sharply peaked around $\bar{n}$. We express the expectation value of the field annihilation operator $\langle a\rangle$ in terms of its amplitude u and phase θ

$$\langle a\rangle = u e^{i\theta}, \tag{13}$$

and, because of our assumptions, $\bar{n}=u^2$.

Using the standard formula for determining the mean value of an operator A, $\langle A\rangle=\mathrm{Tr}\{A\hat{\rho}\}$, and Eq. (11) we are able to obtain the needed equation for $\langle a\rangle$. First, we multiply Eq. (11) by a and then we take the trace with respect to the photon number states. On the left-hand side we then get

$$\mathrm{Tr}\left\{a\frac{d\hat{\rho}}{dt}\right\}=\frac{d}{dt}\mathrm{Tr}\{a\hat{\rho}\}=\frac{d}{dt}\langle a\rangle, \tag{14}$$

since in the Shrödinger picture the operator a does not depend on time. It is easy to resolve the loss term on the right-hand side of Eq. (11) employing the cyclic property of the trace

$$\langle aL\rangle=\frac{1}{2}\gamma\,\mathrm{Tr}\{[a^\dagger,a]a\hat{\rho}\}=-\frac{\gamma}{2}\langle a\rangle, \tag{15}$$

if Eq. (9) is considered, while proceeding with the first term is a little bit more involved. The term

$$\mathrm{Tr}\{a(M-1)\hat{\rho}\}=\langle a(M-1)\rangle \tag{16}$$

can be expressed in the form

$$\begin{aligned}\langle a(\hat{M}-1)\rangle=\sum_{n=0}^{\infty}\sqrt{n+1}\{&\rho_{n+1,n}(|\alpha|^2c_{n+2}c_{n+1}\\&+|\beta|^2c_{n+1}c_n-1)+\rho_{n,n-1}|\alpha|^2s_{n+1}s_n\\&+\rho_{n+2,n+1}|\beta|^2s_{n+2}s_{n+1}\\&+i\alpha\beta^*(c_{n+2}s_{n+1}\rho_{n+1,n+1}-s_{n+1}c_n\rho_{nn})\\&+i\alpha^*\beta(c_{n+1}s_n\rho_{n+1,n-1}-s_{n+2}c_{n+1}\rho_{n+2,n})\}.\end{aligned} \tag{17}$$

Equation (17) can be further approximated by taking into account the fact that we deal with a field whose number distribution is sharply peaked at $\bar{n}$, where $\bar{n}\gg 1$. Namely, we restrict our attention to field density matrices, which have only a few nonzero elements: $\rho_{\bar{n}\bar{n}}$ and those nearby, Fig. 2. Then in the sum in Eq. (17) only those terms will contribute that include the density matrix elements $\rho_{n_1n_2}$, where n_1 and n_2 are close to $\bar{n}$. We also use the Taylor expansion with respect to n, keeping only terms up to the order of $1/\sqrt{\bar{n}}$, to evaluate s_{n+1} and c_{n+1} in terms of s_n and c_n, respectively. For s_{n+1} and c_{n+1} we then get

$$s_{n+1}\approx s_n+\frac{ds_n}{dn}, \tag{18}$$

$$c_{n+1}\approx c_n+\frac{dc_n}{dn}, \tag{19}$$

the derivatives of s_n and c_n can be found with the help of Eqs. (6) and (7), $ds_n/dn=\theta_{\rm int}c_n/2\sqrt{nN_{\rm ex}}$ and $dc_n/dn=-\theta_{\rm int}s_n/2\sqrt{nN_{\rm ex}}$, respectively. Finally, if we put together what we have, we get

$$\frac{d\langle a\rangle}{dt}=r\sum_{n=0}^{\infty}\left\{\frac{1}{2\sqrt{n}}(|\alpha|^2-|\beta|^2)s_n^2\rho_{n,n-1}+i\alpha\beta^*\times\left(-\frac{\theta_{\rm int}}{2\sqrt{N_{\rm ex}}}-\frac{s_nc_n}{2\sqrt{n}}\right)\rho_{nn}-i\alpha^*\beta\times\left(\frac{\theta_{\rm int}}{2\sqrt{N_{\rm ex}}}-\frac{s_nc_n}{2\sqrt{n}}\right)\rho_{n+1,n-1}\right\}-\frac{\gamma}{2}\langle a\rangle. \tag{20}$$

We expect the steady-state micromaser field to be close to a coherent state $|\eta\rangle$, where $\eta=\langle a\rangle$ and $|\eta|^2=\overline{n}$, which has the density matrix in the number-state representation

$$\rho_{mn}=e^{-|\eta|^2}\frac{(\eta^*)^n\eta^m}{\sqrt{m!n!}}. \tag{21}$$

Therefore, the nondiagonal density matrix elements in Eq. (20) can be expressed as

$$\frac{\eta^*}{\sqrt{n}}\rho_{n,n-1}=\rho_{nn} \tag{22}$$

and

$$\rho_{n+1,n-1}=\frac{\eta}{\sqrt{n+1}}\frac{\sqrt{n}}{\eta^*}\rho_{nn}. \tag{23}$$

Keeping in mind that ρ_{nn} is sharply peaked about $\overline{n}$, this implies that Eq. (20) can be put into the form

$$\frac{d(ue^{i\theta})}{dt'}=N_{\rm ex}\left\{\frac{1}{2u}(|\alpha|^2-|\beta|^2)s_{\overline{n}}^2e^{i\theta}+|\alpha\beta|e^{i\phi}\times\left(-\frac{\theta_{\rm int}}{2\sqrt{N_{\rm ex}}}-\frac{s_{\overline{n}}c_{\overline{n}}}{2u}\right)-|\alpha\beta|e^{-i\phi}\times\left(-\frac{\theta_{\rm int}}{2\sqrt{N_{\rm ex}}}+\frac{s_{\overline{n}}c_{\overline{n}}}{2u}\right)e^{2i\theta}\right\}-\frac{1}{2}ue^{i\theta}. \tag{24}$$

We have defined a new time parameter $t'=\gamma t$, and set

$$i\alpha\beta^*=|\alpha\beta|e^{i\phi}. \tag{25}$$

Equation (24) can now be solved for the two real variables u and θ. The steady-state values of u and θ are determined by setting the time derivative equal to zero. For the phase θ of the steady-state field, two solutions are possible as one can easily verify: $\theta=\phi$ and $\theta=\phi+\pi$. However, as long as we are in the classical regime, we expect that only one is physical. We will resort to a stability analysis to determine which one is stable, i.e., physically realizable, and which one is merely formal.

IV. STABILITY ANALYSIS

As it was said in the previous section, Eq. (24) can be solved for the steady-state values of $\overline{n}=u^2$ and θ. Using either solution of the phase θ we will get a transcendental equation for the mean photon number $\overline{n}=\overline{n}(\theta_{\rm int})$ as a function of the pumping parameter $\theta_{\rm int}$. In order to determine whether the solution is stable we will displace the system from its steady state by $\delta\theta$ and δu, $\delta\theta\ll\theta$, and $\delta u\ll u$, respectively. If the system shows a tendency to move towards its steady state in both variables [in an abstract sense the system is moving in the (u,θ) plane], the solution is stable, and vice versa.

A. Unstable solution

Let us first examine the case

$$\theta=\phi. \tag{26}$$

This is substituted into Eq. (24) which gives us the equation for $\overline{n}(\theta_{\rm int})$ at steady state,

$$0=(|\alpha|^2-|\beta|^2)s_{\overline{n}}^2-2|\alpha\beta|s_{\overline{n}}c_{\overline{n}}-\frac{\overline{n}}{N_{\rm ex}}. \tag{27}$$

In order to find the stable points, we change $\theta\to\theta+\delta\theta$ and $u\to u+\delta u$ in Eq. (24). We then employ a Taylor expansion to find both sides up to first order in $\delta\theta$ and δu. We obtain the expression for the time derivative of δu from the real part of the resulting equation,

$$\delta\dot{u}=\left\{\frac{\theta_{\rm int}\sqrt{N_{\rm ex}}}{u}[(|\alpha|^2-|\beta|^2)c_{\overline{n}}s_{\overline{n}}+|\alpha\beta|(s_{\overline{n}}^2-c_{\overline{n}}^2)]-1\right\}\delta u, \tag{28}$$

while from the imaginary part we have

$$\delta\dot{\theta}=|\alpha\beta|\frac{\theta_{\rm int}\sqrt{N_{\rm ex}}}{u}\delta\theta. \tag{29}$$

All terms on the right-hand side of the last equation are positive real numbers, so that they form a positive factor multiplying $\delta\theta$. Then $\dot{\delta\theta}$ (we may say it is the ''velocity'' of $\delta\theta$) always has the same direction as $\delta\theta$. That means the phase of the system at the point $(u+\delta u,\theta+\delta\theta)$ is moving away from θ, see Fig. 3(a). Therefore, all points (u,θ), which we obtain from Eq. (27), are not stable.

B. Stable solution

If we repeat the procedure for

$$\theta=\phi+\pi, \tag{30}$$

then we find

$$0=(|\alpha|^2-|\beta|^2)s_{\overline{n}}^2+2|\alpha\beta|s_{\overline{n}}c_{\overline{n}}-\frac{\overline{n}}{N_{\rm ex}} \tag{31}$$

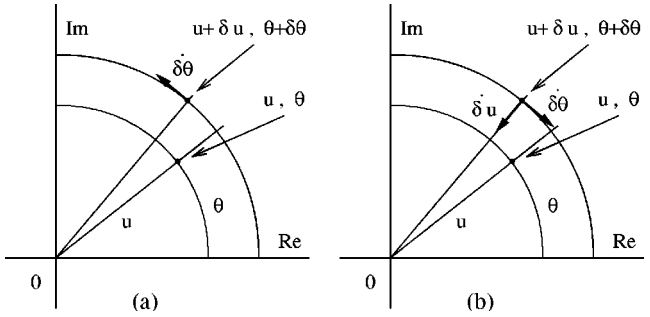

FIG. 3. Solutions of Eq. (24) for the complex amplitude $\eta = ue^{i\theta}$ are represented via polar coordinates u, θ. (a) Shows nonstable case for $\theta=\phi$, the ''velocity'' $\dot{\delta}\theta$ has the same direction as the displacement $\delta\theta$. (b) Shows stable points (u,θ) for the situation when $\theta=\phi+\pi$ since both $\dot{\delta}u$ and $\dot{\delta}\theta$ at point $(u+\delta u,\ \theta+\delta\theta)$ point back towards (u,θ).

as the equation for $\bar{n}(\theta_{\rm int})$, and, for the equations of motion for δu and $\delta\theta$,

$$\dot{\delta u}=\left\{\frac{\theta_{\rm int}\sqrt{N_{\rm ex}}}{u}[(|\alpha|^2-|\beta|^2)c_{\bar{n}}s_{\bar{n}}-|\alpha\beta|(s_{\bar{n}}^2-c_{\bar{n}}^2)]-1\right\}\delta u, \tag{32}$$

$$\dot{\delta\theta}=-|\alpha\beta|\frac{\theta_{\rm int}\sqrt{N_{\rm ex}}}{u}\delta\theta. \tag{33}$$

As one can see, the factor multiplying $\delta\theta$ in Eq. (33) has a negative sign. Therefore, the system has a tendency to move from the state with phase $\theta+\delta\theta$ back to θ. However, we still have to check the behavior of $\dot{\delta u}$ in order to determine whether the point (u,θ) is stable. It is hard to see by inspection of Eq. (32) what the direction of $\dot{\delta u}$ is. We need the term in the curly brackets to be negative for the field to be at stable (u,θ), see Fig. 3(b). The sign of this factor and the stable solutions can be found numerically. These results were compared with those from numerical simulations and this will be presented shortly. Now, however, we want to turn our attention to the problem of finding the phase distribution of the steady-state field.

V. PHASE DISTRIBUTION

Knowing the field density matrix at given time the phase distribution of the field can be calculated. The probability that the phase is within the interval $\lambda,\lambda+d\lambda$ is $\langle\lambda|\hat{\rho}|\lambda\rangle d\lambda$, where $|\lambda\rangle$ is the quantum-mechanical phase state

$$|\lambda\rangle\equiv\frac{1}{\sqrt{2\pi}}\sum_{n=0}^{\infty}e^{in\lambda}|n\rangle. \tag{34}$$

Therefore, the phase distribution is defined by the diagonal density matrix elements $\langle\lambda|\hat{\rho}|\lambda\rangle$. The core of our approach to determining the phase distribution lies in using the special orthogonal atomic states

$$|\pm\rangle\equiv\frac{1}{\sqrt{2}}(e^{-i\varphi}|a\rangle\pm|b\rangle), \tag{35}$$

as the atomic basis. These states are actually the eigenstates of the semiclassical interaction Hamiltonian, which is obtained by replacing the operators a ($a^\dagger$) in the interaction term of Eq. (1) by the c-number field amplitude v (v^*), $v=|v|e^{-i\varphi}$,

$$H_{\rm int,sc}=g(\sigma^- v^*+\sigma^+ v). \tag{36}$$

The dynamics of these states was intensively studied within the contex of the Jaynes-Cummings model by Gea-Banacloche [15] who discovered a formula that describes their time evolution in the limit of large photon number $\bar{n}$. On a time scale that is much smaller than the revival time $t_r=2\pi\sqrt{\bar{n}}/g$, if the micromaser field is prepared in the coherent state $|v\rangle$, where $v=\sqrt{\bar{n}}e^{-i\varphi}$, then $|\pm\rangle|v\rangle$ evolves as

$$|\pm\rangle|v\rangle\rightarrow e^{\mp i(gt\sqrt{\bar{n}}/2)}|\pm\rangle|ve^{\mp i(gt/2\sqrt{\bar{n}})}\rangle. \tag{37}$$

The error in Eq. (37) is of order $1/\sqrt{\bar{n}}$. This result provides a convenient way of treating the systems with large photon number, because the total state vector remains a product of the atomic and field parts.

An arbitrary atomic state can be expressed as

$$|\Psi\rangle=e^{-iw}\sin\kappa|a\rangle+\cos\kappa|b\rangle, \tag{38}$$

which in the basis of $|\pm\rangle$ states becomes

$$|\Psi\rangle=\langle+;\varphi|\Psi\rangle|+;\varphi\rangle+\langle-;\varphi|\Psi\rangle|-;\varphi\rangle, \tag{39}$$

where the explicit phase dependence of states $|\pm\rangle$ has been included. The coefficients of this expansion can be found easily

$$|\langle+;\varphi|\Psi\rangle|^2=\frac{1}{2}[1+\cos(w-\varphi)\sin(2\kappa)],$$

$$|\langle-;\varphi|\Psi\rangle|^2=\frac{1}{2}[1-\cos(w-\varphi)\sin(2\kappa)]. \tag{40}$$

For any initial atomic state $|\Psi\rangle$, Eq. (37) can be employed for finding the total state of the system at later time. We are concerned with the steady-state micromaser field, and its phase in particular, therefore we shall need the evolution of the field density matrix $\hat{\rho}$. The initial density matrix of the system $\hat{\rho}_{\rm system}=|v\rangle|\Psi\rangle\langle\Psi|\langle v|$ evolves in time according Eq. (37) too, of course, and it provides the field density operator after we take the trace with respect to the atomic degrees of freedom. We obtain

$$|v\rangle\langle v|\rightarrow|\langle+;\varphi|\Psi\rangle|^2|e^{-i\delta\varphi}v\rangle\langle e^{-i\delta\varphi}v| + |\langle-;\varphi|\Psi\rangle|^2|e^{i\delta\varphi}v\rangle\langle e^{i\delta\varphi}v|, \tag{41}$$

where $\delta\varphi=g\tau/2\sqrt{\bar{n}}$. In order to find the steady-state phase distribution of the field, the P representation of the density

matrix may be used. The P representation is a diagonal representation of $\hat{\rho}$ in terms of coherent states, $|\xi\rangle$, as $\hat{\rho} = \int d^2\xi P(\xi)|\xi\rangle\langle\xi|$. Using this, we can convert Eq. (41) into an equation for $P(v)$

$$P(v) \rightarrow |\langle\Psi|+;\varphi-\delta\varphi\rangle|^2 P(ve^{i\delta\varphi}) + |\langle\Psi|-;\varphi+\delta\varphi\rangle|^2 P(ve^{-i\delta\varphi}). \tag{42}$$

It is apparent that Eq. (42) describes merely changes of the field phase, the field amplitude is unaffected, so that we drop the explicit $|v|$ dependence in $P(|v|e^{-i\varphi})$. With the help of Eq. (40) we find

$$P(\varphi) \rightarrow \frac{1}{2}[1+\cos(w-\varphi+\delta\varphi)\sin 2\kappa]P(\varphi-\delta\varphi) + \frac{1}{2}[1-\cos(w-\varphi-\delta\varphi)\sin 2\kappa]P(\varphi+\delta\varphi). \tag{43}$$

The right-hand side of Eq. (43) must be equal to $P(\varphi)$ for the steady-state field. For a large $\bar{n}$ we have $\delta\varphi \ll 1$, therefore we expand the right-hand side of Eq. (43) up to the second order of $\delta\varphi$ and then the steady-state condition gives us the second-order differential equation for $P(\varphi)$

$$0 = -\frac{d}{d\varphi}[P(\varphi)\cos(w-\varphi)\sin 2\kappa] + \frac{1}{2}\frac{d^2}{d\varphi^2}P(\varphi)\delta\varphi. \tag{44}$$

This can be integrated giving the periodic solutions

$$P(\varphi) = C' e^{-(2\sin 2\kappa/\delta\varphi)\sin(w-\varphi)}, \tag{45}$$

where C' is the constant of integration. Note, that even though the formal solution to Eq. (44) has two constants, one of them is eliminated by the requirement of periodicity. The solutions given by Eq. (45) allow us to draw several conclusions. First, without even knowing C', one can immediately find the position of the maximum of the phase distribution

$$\varphi_{\max} = w - \frac{3\pi}{2}. \tag{46}$$

Second, the phase probability distribution $R(\lambda) \equiv \langle\lambda|\hat{\rho}|\lambda\rangle$ can be calculated from

$$R(\lambda) = \int d^2\xi P(\xi)|\langle\xi|\lambda\rangle|^2. \tag{47}$$

The coherent state in the number-state representation is defined as

$$|\xi\rangle \equiv e^{-|\xi|^2/2}\sum_{n=0}^{\infty}\frac{\xi^n}{\sqrt{n!}}|n\rangle, \tag{48}$$

and then from Eq. (47) we obtain final expression for $R(\lambda)$ ($r = \sqrt{\bar{n}}$)

$$R(\lambda) = \frac{C}{2\pi}e^{-r^2}\sum_{n,m=0}^{\infty}\frac{r^{m+n}}{\sqrt{m!n!}}\int_0^{2\pi}d\varphi\cos[(\varphi+\lambda) \times (n-m)]e^{-(2\sin 2\kappa/\delta\varphi)\sin(w-\varphi)}. \tag{49}$$

The constant C is determined from the normalization condition

$$\int_0^{2\pi} R(\lambda)d\lambda = 1. \tag{50}$$

The integral with respect to λ is

$$\int_0^{2\pi} d\lambda \cos((\varphi+\lambda)(n-m)) = 2\pi\delta_{nm}, \tag{51}$$

where δ_{nm} is the Kronecker symbol, so that we have finally

$$C = \left[\int_0^{2\pi} d\varphi e^{-(2\sin 2\kappa/\delta\varphi)\sin(w-\varphi)}\right]^{-1}. \tag{52}$$

The results from the numerical simulations, which are presented in the following section, show that Eq. (49) is very precise when $\bar{n}$ is large.

VI. NUMERICAL RESULTS

In most of the following numerical experiments the atom-field interaction constant g was 4.4×10^4 Hz and the relative phase of the coherent atomic state u [as defined by Eq. (38)] was set to 0. The pumping statistics was chosen to be regular, because the Poissonian case is computationally very demanding. We shall comment on the effect this has on our results shortly.

We studied how the steady-state field varies with respect to the micromaser parameters $N_{\rm ex}$, $\theta_{\rm int}$, and $|\alpha|$. In Fig. 4 we plot the mean photon number $\bar{n}$ in the steady state as a function of $\theta_{\rm int}$ when $N_{\rm ex}=30$ and $|\alpha|=0.9$. The $\theta_{\rm int}$ interval was evenly sampled by 201 points between 0 and 40. For each value of $\theta_{\rm int}$ we found $\bar{n}$ performing the following procedure. The initial state of the cavity field was taken to be the vacuum. The field then interacted with an atom according to Eq. (8), and then decayed according to Eq. (10). The measurement of the field's mean photon number $\bar{n}$ was performed just before the next atom entered the cavity. This sequence, corresponding to Eq. (12), was repeated until the steady-state value of $\bar{n}$ was found. The field was considered steady when its $\bar{n}$ changed by less than 10^{-3}% during a single sequence. The reason behind this is that we had to set an upper bound for the number of interactions in order to get the results in reasonable time; for smaller $N_{\rm ex}$ (30 to 100) it was set to $30N_{\rm ex}$ and for larger $N_{\rm ex}$ it was $15N_{\rm ex}$. If $\bar{n}$ changes at a rate of 10^{-3}% per sequence, then the field would need to interact with 10^5 atoms to increase its value by one. This means that such small differences would not show up on the graphs, even if we considered the maximum number of interactions to be 7500 ($N_{\rm ex}=500$).

The points from the quantum-mechanical simulations are

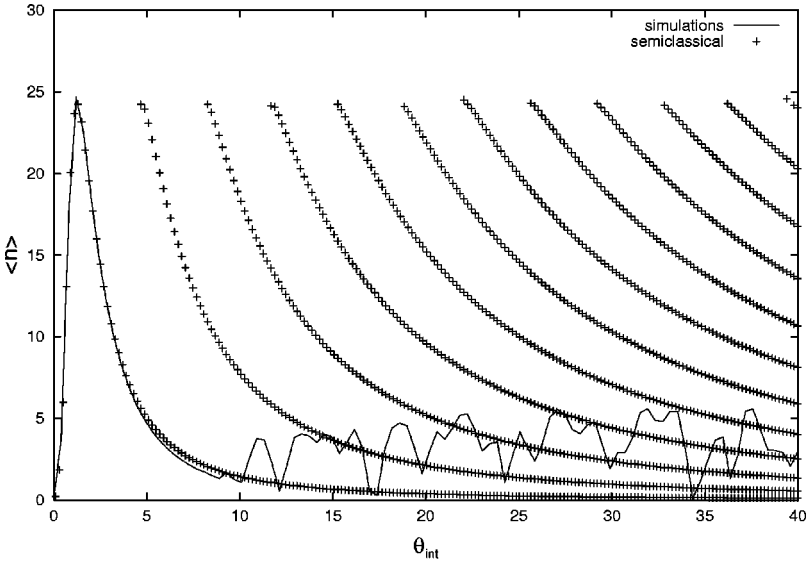

FIG. 4. Mean photon number $\overline{n}$ of the steady-state field vs the pumping parameter $\theta_{\rm int}$, $|\alpha|=0.9$ and $N_{\rm ex}=30$. The points from the quantum-mechanical simulations with regular pumping are joined by the continuous line, while the crosses show semiclassical stable solutions where Poissonian pumping was assumed.

in Fig. 4 are joined by a continuous line. The crosses on the same figure show semiclassical stable solutions as given by Eq. (31). We find a very good correspondence between the two when $\theta_{\rm int}$ is between 0 and 5. The two curves are almost identical in the vicinity of the first micromaser threshold where $\overline{n}$ has its maximum. The quantum-mechanical line shows the second threshold around $\theta_{\rm int}=10$, and beyond this point it does not match the semiclassical pattern. The relationship between $\overline{n}$ and $\theta_{\rm int}$ was also studied for $N_{\rm ex}=100$, 300, and 500; the results are shown in Figs. 5, 6, 7. As $N_{\rm ex}$ increases the second threshold moves to larger values of $\theta_{\rm int}$, for example, when $N_{\rm ex}=500$ it occurs around $\theta_{\rm int}=37$, while the quantum-mechanical and the semiclassical solutions coincide for larger intervals of $\theta_{\rm int}$. Therefore, we may conclude that our semiclassical theory gives correct predictions for $\overline{n}(\theta_{\rm int})$ provided that $N_{\rm ex}$ is large.

We were also concerned with the questions of how $\overline{n}(\theta_{\rm int})$ and the relationship between the quantum-mechanical and the semiclassical solutions depend on $|\alpha|$. To answer this question four simulations were done setting $|\alpha|$ to 0.85, 0.9, 0.95, and 1.0 with $N_{\rm ex}=300$. The results are plotted in Figs. 8, 6, 9, 10. As one can see, the second threshold occurs at smaller $\theta_{\rm int}$ as $|\alpha|$ increases. Up to that point the quantum-mechanical and the semiclassical curves are almost identical.

A careful reader has probably noticed that we were using different pumping statistics for the semiclassical theory and for the numerical simulations. He may ask whether our comparison is reasonable and how much the results of the semiclassical theory depend on the pumping statistics. In order to investigate this point we shall find the semiclassical stable solutions for the amplitude and the phase of the steady-state field for a micromaser with regular pumping. If it is assumed that the measurements are performed just before the pumping atoms enter the cavity, Fig. 1(a), then the steady-state condition gives

$$\langle a(t_{i+1})\rangle=\langle a(t_i)\rangle, \tag{53}$$

which can be expressed with the help of Eq. (12) as

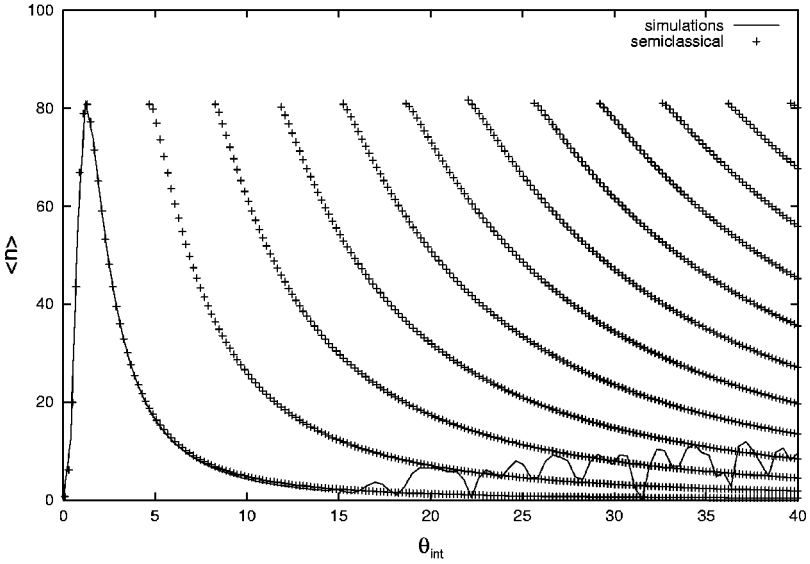

FIG. 5. Mean photon number $\overline{n}$ of the steady-state field vs the pumping parameter $\theta_{\rm int}$, $|\alpha|=0.9$ and $N_{\rm ex}=100$. The points from the quantum-mechanical simulations with regular pumping are joined by the continuous line, while the crosses show semiclassical stable solutions where Poissonian pumping was assumed.

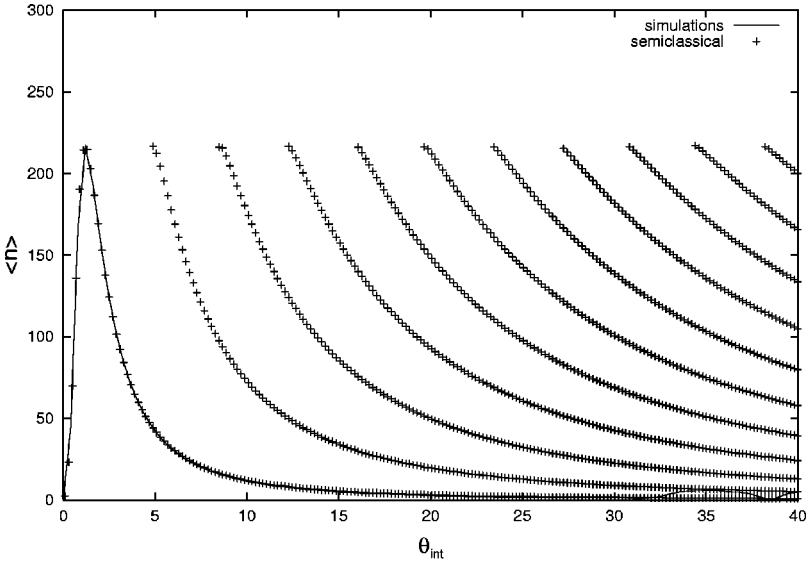

FIG. 6. Mean photon number $\bar{n}$ of the steady-state field vs the pumping parameter $\theta_{\rm int}$, $|\alpha|=0.85$ and $N_{\rm ex}=300$. The points from the quantum-mechanical simulations with regular pumping are joined by the continuous line, while the crosses show semiclassical stable solutions where Poissonian pumping was assumed.

$$\mathrm{Tr}\{e^{LT}M\hat{\rho}(t_i)a\}=\mathrm{Tr}\{\hat{\rho}(t_i)a\}. \tag{54}$$

Following the procedure from Secs. III and IV, we find that the phase θ of the steady-state field is

$$\theta=\phi+\pi, \tag{55}$$

and the amplitude of the field can be determined from

$$u-u'=\frac{1}{2u'}(|\alpha|^2-|\beta^2|)s_{\bar{n}'}^2+|\alpha\beta|\frac{s_{\bar{n}'}c_{\bar{n}'}}{u'}, \tag{56}$$

where

$$u'=e^{-1/2N_{\rm ex}}u. \tag{57}$$

The same notation as in Eqs. (13), (25) was used. The stability analysis gives us time evolution of δn and $\delta\theta$ in terms of the maps

$$\delta u\rightarrow\frac{1}{u}\left[2u'-u+\{(|\alpha|^2-|\beta|^2)s_{\bar{n}'}c_{\bar{n}'}+|\alpha\beta|(c_{\bar{n}'}^2-s_{\bar{n}'}^2)\}\frac{\theta_{\rm int}}{\sqrt{N_{\rm ex}}}\right]\delta u, \tag{58}$$

$$\delta\theta\rightarrow\left[1-|\alpha\beta|\frac{\theta_{\rm int}}{u\sqrt{N_{\rm ex}}}\right]\delta\theta. \tag{59}$$

We have plotted the stable points for the case with $|\alpha|=1.0$ and $N_{\rm ex}=300$ in Fig. 10, and we see that they come very close to those calculated with Poissonian pumping. We further find that the points for both kinds of pumping statistics stay close for large $N_{\rm ex}$, and they only start to differ as

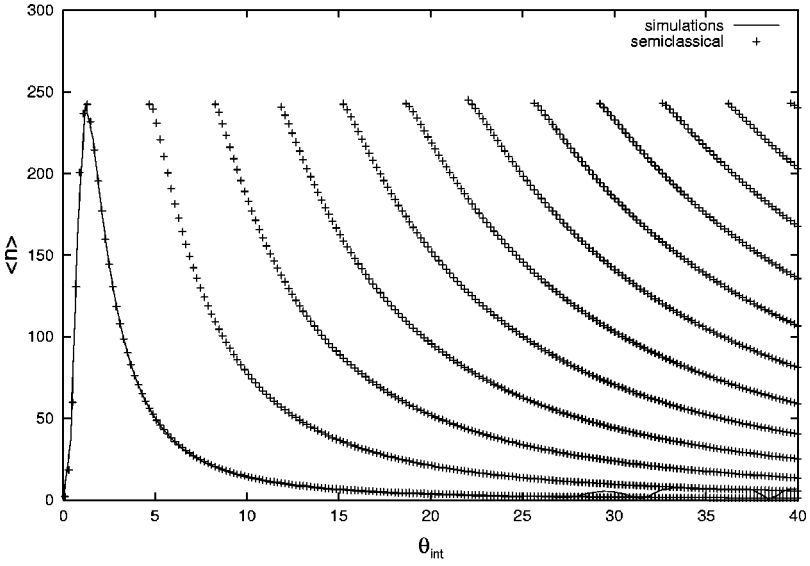

FIG. 7. Mean photon number $\bar{n}$ of the steady-state field vs the pumping parameter $\theta_{\rm int}$, $|\alpha|=0.9$ and $N_{\rm ex}=300$. The points from the quantum-mechanical simulations with regular pumping are joined by the continuous line, while the crosses show semiclassical stable solutions where Poissonian pumping was assumed.

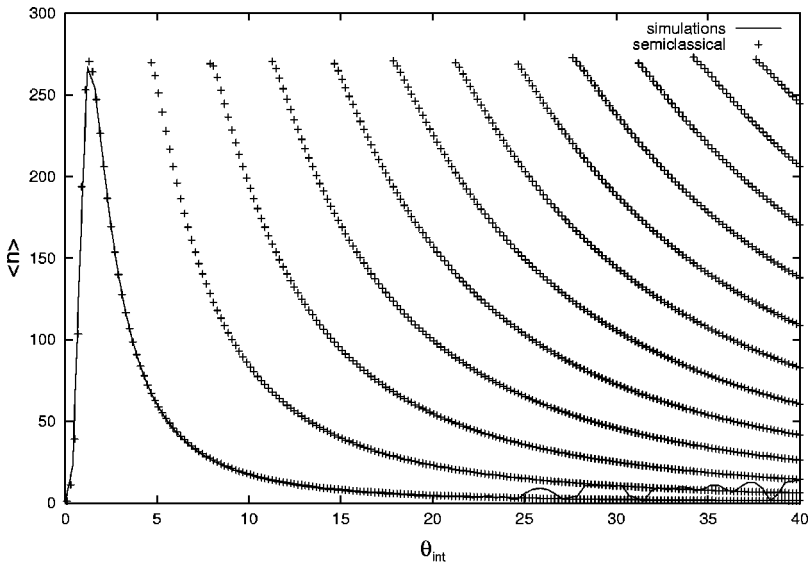

FIG. 8. Mean photon number $\bar{n}$ of the steady-state field vs the pumping parameter $\theta_{\rm int}$, $|\alpha|=0.95$ and $N_{\rm ex}=300$. The points from the quantum-mechanical simulations with regular pumping are joined by the continuous line, while the crosses show semiclassical stable solutions where Poissonian pumping was assumed.

$\theta_{\rm int}$ increases. However, even for small $N_{\rm ex}$ (such as 30) they both provide almost the same values of $\bar{n}$ for $\theta_{\rm int}$ around the first threshold, which is also in very good correspondence with the quantum-mechanical simulations, Fig. 10. Therefore we conclude that the pumping statistics does not play a role in the semiclassical treatment of the micromaser if the objective is to determine the mean photon number of the steady-state field for values of $\theta_{\rm int}$ of order 1. We prefer to work with Poissonian pumping because it corresponds better to the actual physical experiments.

The next question we would like to ask is will the pumping statistics make a bigger difference in the quantum-mechanical treatment of the micromaser? The probabilities p_n of the steady-state field having n photons for the micromaser with Poissonian pumping can be found analytically [19]

$$p_n = p_0 \prod_{m=1}^{n} \frac{\rho_{aa} s_m^2}{\rho_{bb} s_m^2 + m/N_{\rm ex}}, \tag{60}$$

where p_0 is determined from the normalization condition

$$\sum_{n=0}^{\infty} p_n = 1. \tag{61}$$

This formula is valid for the situation when the pumping atoms are in the mixed state: $\rho_{aa}|a\rangle\langle a| + \rho_{bb}|b\rangle\langle b|$. The formula was used for calculating $\bar{n}(\theta_{\rm int})$, Fig. 11. We set $\rho_{aa}=1$ in order to compare the resulting points to our simulations (note that we use pure atomic states there). The figure shows the apparent second, third, and higher thresholds where, according to the analogy with statistical physics, the micromaser field undergoes the first-order phase transition. Comparing with Figs. 10 and 11, we see that the curves corresponding to the quantum-mechanical results for regular and Poissonian pumping are very different, they coincide around the first threshold only. Therefore, the pumping statistics does have remarkable effect in the quantum-mechanical theory.

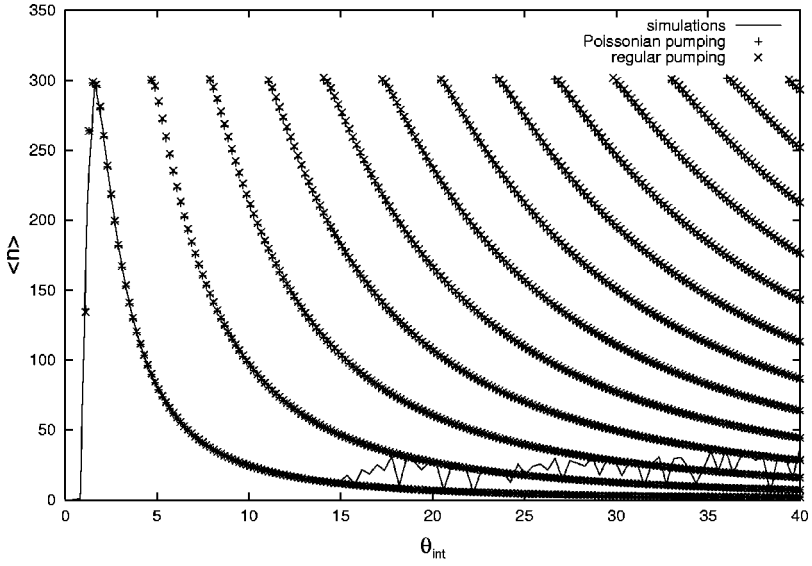

FIG. 9. $\bar{n}$ vs $\theta_{\rm int}$ for the case with $|\alpha|=1.0$ and $N_{\rm ex}=300$. The continuous line joins the steady-state points gained from the quantum-mechanical simulation with regular pumping. The two types of crosses now show *semiclassical* stable solutions for both Poissonian and regular pumping. For larger values of $N_{\rm ex}$ the two almost coincide.

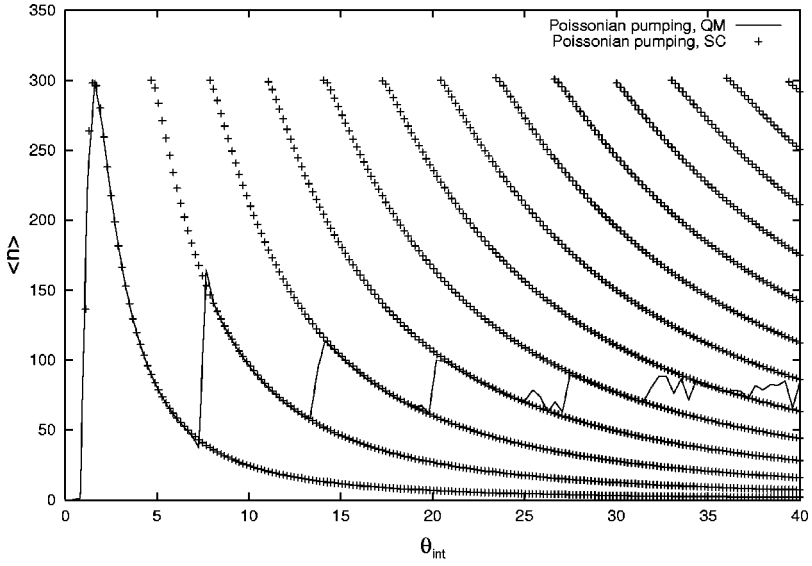

FIG. 10. $\overline{n}$ vs $\theta_{\rm int}$ for the case with $|\alpha|=1.0$ and $N_{\rm ex}=300$. The continuous line now represents analytical *quantum-mechanical* solutions for Poissonian pumping. The crosses stand for the semiclassical stable points. The quantum-mechanical curve is quite different from the previous cases with regular pumping.

So far, it was found that the semiclassical predictions agree very well with the quantum-mechanical simulations in the region around the first threshold where the mean photon number reaches its maximum values. It was supposed in the analytical treatment that the steady-state field is coherent, for which $\overline{n}=|\eta|^2$ and the root-mean-squared deviation of the photon distribution $\sigma=|\eta|$, where η is its amplitude. We can examine this assumption by calculating the values of $\sigma/\sqrt{\overline{n}}$ and $|\langle a\rangle|^2/\overline{n}$ as a functions of $\theta_{\rm int}$, and these are plotted in Fig. 12 for the steady-state field of the micromaser with $N_{\rm ex}=300$ and $|\alpha|=0.9$. Both curves are smooth on the region between 0 and 15 approximately, which corresponds to the area around the first threshold. The values of $|\langle a\rangle|^2/\overline{n}$ are close to 1, also $\sigma/\sqrt{\overline{n}}$ is almost constant on the largest portion of the region though smaller than 1. Therefore, our assumption about the strong steady-state micromaser field is justified, indeed.

At last, we want to check the validity of Eq. (49). We present results from two simulations; in both cases $|\alpha|=0.9$ and $w=0$. Figure 13 shows the phase distribution of the steady-state field for $N_{\rm ex}=30$; it was chosen so that $\theta_{\rm int}=1.12$ since it provides large mean photon number, $\overline{n}=23.6$, which gives $\delta\varphi=0.0253$. The values of $\delta\varphi$ and $\overline{n}$ were used when calculating the distribution from Eq. (49), where we set the upper limit for the indices m, n to 50. The resulting curve matches very well the phase distribution from the numerical simulations. We find some differences only at the tip of the peak where the analytical one is slightly taller, approximately by 5%. The second comparison, Fig. 14, is for the situation when $N_{\rm ex}=100$, $\theta_{\rm int}=1.2$, and $\overline{n}=80.3$ for which $\delta\varphi=6.70\times10^{-3}$. Also here the analytical distribution agrees very well with the numerical simulations. The peak is narrower and we see some differences only at its tip. Experimenting more with the parameters it was found that Eq. (49) provides excellent results for large $\overline{n}$; values of $\overline{n}$ as small as 15 provide good agreement. For $\theta_{\rm int}$ where $\overline{n}$ was smaller, the peak became less pronounced and the values started to depart from those obtained from the simulations.

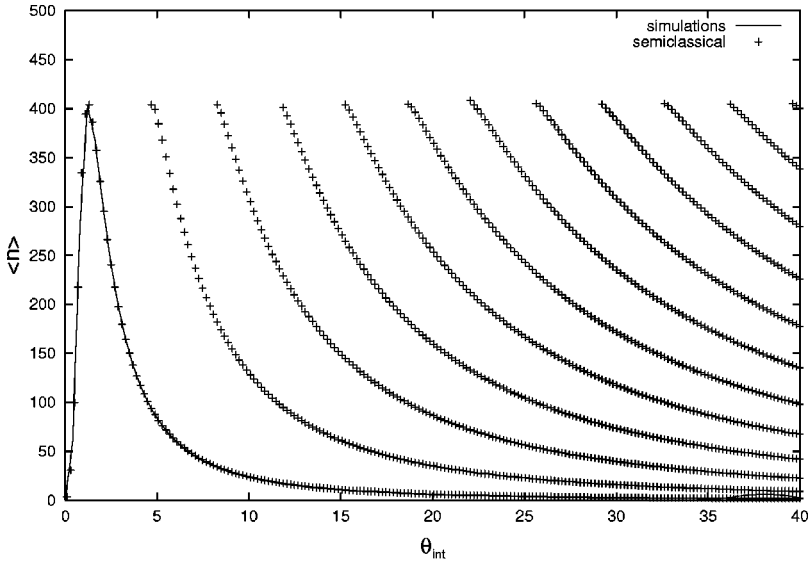

FIG. 11. Mean photon number $\overline{n}$ of the steady-state field vs the pumping parameter $\theta_{\rm int}$, $|\alpha|=0.9$ and $N_{\rm ex}=500$. The points from the quantum-mechanical simulations with regular pumping are joined by the continuous line, while the crosses show semiclassical stable solutions where Poissonian pumping was assumed.

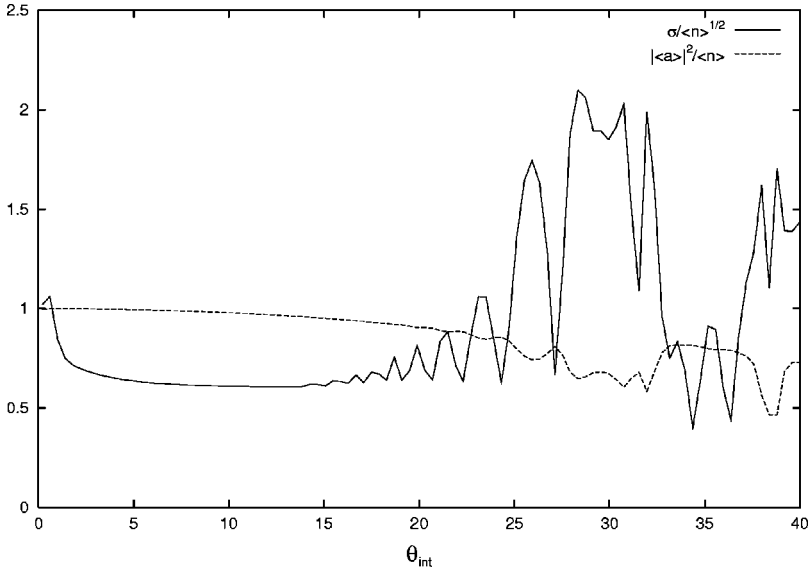

FIG. 12. The normalized root-mean-squared deviation $\sigma/\sqrt{\overline{n}}$ of the photon number of the steady-state field vs the pumping parameter θ_{int} is plotted by the continuous line, while the dashed line shows the ratio $|\langle a\rangle|^2/\overline{n}$ vs θ_{int}. Within the approximate interval (0,15) the value is close to 1, which shows that the field is almost coherent. $N_{\text{ex}}=300$ and $|\alpha|=0.9$.

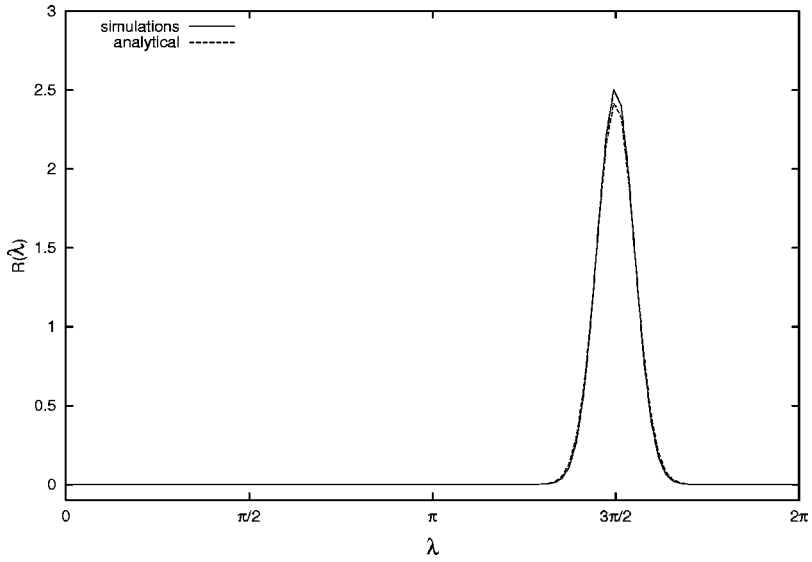

FIG. 13. Phase distribution of the steady-state field. Data from the numerical simulations is shown by the continuous line, the dashed line shows results from Eq. (49). This is the case with $N_{\text{ex}}=30$, $|\alpha|=0.9$, and $\theta_{\text{int}}=1.12$.

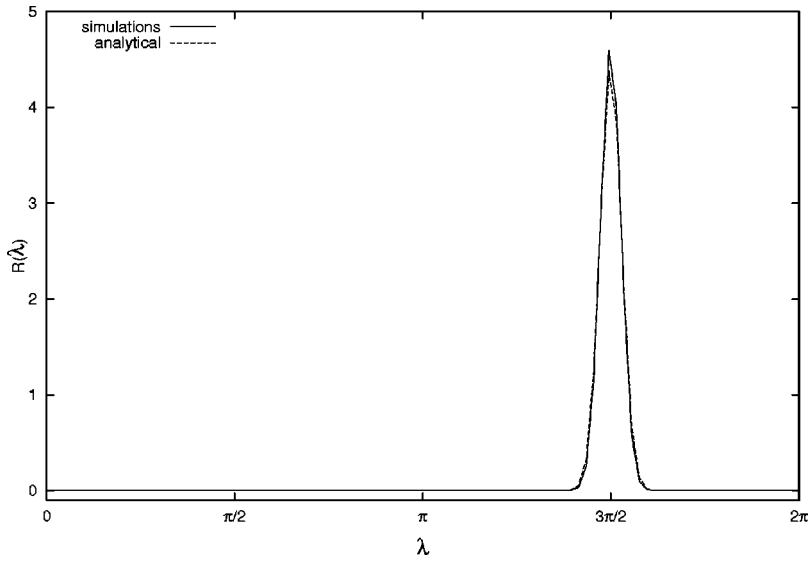

FIG. 14. Phase distribution of the steady-state field. Data from the numerical simulations is shown by the continuous line, the dashed line shows results from Eq. (49). This is the case with $N_{\text{ex}}=100$, $|\alpha|=0.9$, and $\theta_{\text{int}}=1.2$.

VII. CONCLUSIONS

Our semiclassical theory provides results that are in very good agreement with the quantum-mechanical numerical simulations when the cavity field has a large mean photon number. The stable solutions for the mean photon number as a function of the interaction parameter $\theta_{\rm int}$ coincide with the simulations on the interval whose size increases as $N_{\rm ex}$ increases while keeping $|\alpha|$ constant. On the other hand, while keeping $N_{\rm ex}$ constant, the interval of validity becomes larger as $|\alpha|$ decreases. The average photon number reaches its maximum, which is equal to $|\alpha|^2 N_{\rm ex}$, at the first threshold. Then as $\theta_{\rm int}$ increases the semiclassical result continues to follow the quantum-mechanical dependence approximately until the latter reaches a second threshold. Also, it was found that the pumping statistics does not play a significant role in the semiclassical treatment if the objective is to determine only the mean photon number. Of course, the same cannot be said about the quantum case.

The semiclassical approximation for the phase distribution is in very good agreement with the quantum-mechanical one. It was shown that it is sufficient to have as few as 15 photons in the steady field to obtain a precise result. The expression for the phase distribution depends on the mean photon number as a parameter. That can be determined using the stable semiclassical solution from Sec. IV. Therefore, the presented theory is complete allowing one to obtain results using only the parameters, such as $N_{\rm ex}$ and $\theta_{\rm int}$, which specify the micromaser.

The present treatment, however, cannot be used to determine the photon number distribution, and this remains a challenge and motivation for further work.

ACKNOWLEDGMENT

One of us (J.S.) wants to thank the Research Foundation of CUNY for partial funding for software used in the numerical simulations.

[1] P. Filipowicz, J. Javanainen, and P. Meystre, Phys. Rev. A **34**, 3077 (1986).
[2] P. Filipowicz, J. Javanainen, and P. Meystre, J. Opt. Soc. Am. B **3**, 906 (1986).
[3] M. Sargent, III, M. O. Scully, and W. E. Lamb, Jr., *Laser Physics* (Addison-Wesley, London, 1974).
[4] A. M. Guzman, P. Meystre, and E. M. Wright, Phys. Rev. A **40**, 2471 (1989).
[5] D. Meschede, H. Walther, and G. Muller, Phys. Rev. Lett. **54**, 551 (1985).
[6] G. Rempe, F. Schmidt-Kaler, and H. Walther, Phys. Rev. Lett. **64**, 2783 (1990).
[7] M. Brune *et al.*, Phys. Rev. Lett. **76**, 1800 (1996).
[8] G. Rempe, H. Walther, and N. Klein, Phys. Rev. Lett. **58**, 353 (1987).
[9] J. Krause, M. O. Scully, and H. Walther, Phys. Rev. A **34**, 2032 (1986).
[10] J. J. Slosser and P. Meystre, Phys. Rev. A **41**, 3867 (1990).
[11] J. Slosser, P. Meystre, and E. Wright, Opt. Lett. **15**, 233 (1990).
[12] J. J. Slosser, P. Meystre, and S. L. Braunstein, Phys. Rev. Lett. **63**, 934 (1989).
[13] M. Hillery and J. Skvarcek, J. Mod. Opt. **45**, 1717 (1998).
[14] F. L. Kien *et al.*, Phys. Rev. A **52**, 3279 (1995).
[15] J. Gea-Banacloche, Phys. Rev. A **44**, 5913 (1991).
[16] W. H. Louisell, *Quantum Statistical Properties of Radiation* (Wiley, New York, 1973).
[17] C. Benkert *et al.*, Phys. Rev. A **41**, 2756 (1990).
[18] U. Herzog and J. A. Bergou, Phys. Rev. A **54**, 5334 (1996).
[19] J. A. Bergou, M. Hillery, and P. Bogar (unpublished).